OPEN ACCESS
JOURNAL OF ADVANCED DIELECTRICS
Vol. 11, No. 3 (2021) 2140001 (6 pages)

DOI: 10.1142/S2010135X21400014

Synthesis and evaluation of nickel cobalt ferrite magnetic ceramics employing two alternative routes

Javier E. Camargo, Leandro A. Ramajo and Miriam S. Castro*

División Cerámicos, INTEMA Instituto de Investigaciones en Ciencia y Tecnología de Materiales (INTEMA, CONICET-UNMdP)
Av. Colón 10850, 7600, Mar del Plata, Argentina

*mcastro@fi.mdp.edu.ar

Received 28 January 2021; Revised 9 March 2021; Accepted 31 March 2021; Published 28 April 2021

$Ni_{0.5}Co_{0.5}Fe_2O_4$ (NCF) powders were obtained employing two alternative synthesis routes: solid-state reaction and Pechini's methods. The ceramic powders were pressed and sintered in the temperature range of 1100 °C to 1250 °C. Microstructural and structural properties were evaluated by SEM, XRD, and Raman spectroscopy. Magnetic hysteresis loops of sintered samples were also recorded. A secondary phase was observed in samples synthesized by Pechini's method, whereas samples obtained by the solid-state reaction method, with the mechanochemical activation of the reagents, only produced the spinel structure. Magnetic properties of samples obtained by the solid-state method displayed higher magnetic saturations and lower coercive fields than those obtained from the Pechini's method.

Keywords: Ferrite; Pechini; Raman spectroscopy; magnetic properties.

1. Introduction

Cobalt ferrite is a well-known hard magnetic material with AB_2O_4 spinel structure, relatively high coercivity (H_c), and magnetic saturation (M_s), while nickel ferrite is a soft magnetic material with both low coercivity and magnetic saturation. Consequently, the combination of these hard and soft ferrites could be useful for a variety of applications.[1–3] Besides, Ni–Co ferrites are frequently employed in electronic devices suitable for high-frequency applications in the telecommunications field. These materials are commercially used in high-quality filters, radio frequency circuits, transformer cores, and read/write heads for high-speed digital tape. The excellent electromagnetic properties of these materials make them suitable for the size reduction of high-frequency application devices.[4]

It is known that the magnetic character of these materials crucially depends on the size and shape of their grains, the purity, and the magnetic stability.[5,6] Therefore, their magnetic properties can be designated by modifications in the starting particle size, selecting the appropriate soft and hard ferrite composition,[6,7] or employing several synthesis methods,[8] according to the specific requirements. Indeed, the complete knowledge of the influence of the synthesis method on the final magnetic properties of these ceramics could improve the device properties.

It is known that magnetic properties can be controlled by using different synthesis methodologies, such as sol–gel,[9] coprecipitation,[10] or hydrothermal routes.[11] Specifically, the auto combustion Pechini's method is a promising route due to the required low processing temperatures, the high-stoichiometry and particle-size control of the products,[12] and the homogeneous starting materials distribution.[13] Nevertheless, considering that many chemical synthesis routes are expensive, the mechanical activated solid-state reaction is an operational technology for the preparation of high amounts of powders.[14] Moreover, a high-energy ball mill is an excellent technique for nanomaterials' synthesis at low temperatures.[15] In all cases, a complete understanding of the synthesis route on the structural, microstructural, and magnetic properties of sintered samples should be achieved.

In this paper, the final properties of $Ni_{0.5}Co_{0.5}Fe_2O_4$ (NCF) magnetic ceramics synthesized by two alternative routes, solid-state reaction and Pechini's methods, are presented and compared. For the complete discussion, structural, microstructural, and magnetic properties are related to the employed synthesis route.

2. Experimental Procedure

Two alternative routes for the NCF synthesis were carried out: the solid-state reaction method, including the mechanochemical activation of the reactants (M1), and the auto combustion Pechini's method (M2).

* Corresponding author.

The reagents for the solid-state reaction method (M1) were $Co(C_2H_3O_2)_2 \cdot 4H_2O$ (p.a. Biopack, Argentina), $Ni(C_2H_3O_2)_2 \cdot 4H_2O$ (Aldrich 99%; Argentina), and Fe_2O_3 (Mallinckrodt 97%, USA). All the reactants were weighted according to the stoichiometric ferrite formula and milled for 6 h in a planetary mill (Fritsch, Pulverisette 7, 900 rpm) using steel jars. The resulting powder was dried at 150 °C for 24 h and calcined at 1050 °C for 2 h. The resulting powder was milled again for 3 h, dried, and sieved.

For Pechini's method (M2), the used reagents were $Ni(NO_3)_2 \cdot 6H_2O$ (Baker 99.8%, USA), $Co(NO_3)_3 \cdot 6H_2O$ (Biopack 98%, Argentina), $Fe(NO_3)_3 \cdot 9H_2O$ (Aldrich 98%, USA), and citric acid (Cicarelli 99%, Argentina). For the synthesis, hexahydrated nickel nitrate, hexahydrated cobalt nitrate, nonahydrated iron nitrate, and citric acid were separately dissolved in water in a solvent ratio of 12.5 mL per 10 mmol solute (H_2O) with a stoichiometric ratio of 0.5:0.5:2:3. All the solutions were separately stirred for 30 min. After that, they were mixed together and ammonium hydroxide was added to maintain the pH = 7. The solution was kept at 200 °C for the auto combustion where a fine black powder was produced. Subsequently, the powder was thermally treated at 850 °C for 2 h to obtain the desired phase.

The ceramic powders obtained by both synthesis methods were uniaxially pressed at 150 MPa into disks of 9 mm diameter and 1 mm thickness. Finally, the pressed samples were sintered at 1100 °C, 1150 °C, 1200 °C, and 1250 °C for 2 h, in an air atmosphere, and employing a heating and cooling rate of 5 °C/min.

The bulk density of the pellets was determined by the Archimedes' method employing distilled water as the immersion medium. The densification degree was calculated taking into account the measured bulk density and the theoretical density of the material. The crystalline structure and microstructure of the sintered samples were characterized by X-ray diffraction (XRD, PANalytical, X'pert Pro, CuKα), scanning electron microscopy (SEM, JEOL 6460LV), and Raman spectroscopy (Renishaw inVia microscope using a 514 nm laser Ar-ion), respectively. Deconvolution and curve fitting of the Raman spectra were achieved with Fityk software using Lorentzian functions after performing a background correction.

Before the observation by SEM, samples were mirror polished and heat treated at 50 °C below the sintering temperature for 20 min. Magnetization, at room temperature and as a function of the magnetic field, was measured by a vibrating sample magnetometer (Lakeshore 7300). The magnetic hysteresis loops were taken between +15 and −15 kOe at room temperature.

3. Results and Discussion

Figure 1 shows the X-ray diffraction spectra of the samples (obtained by both methods) sintered between 1100 °C and 1250 °C for 5 h. XRD patterns confirm that the NCF

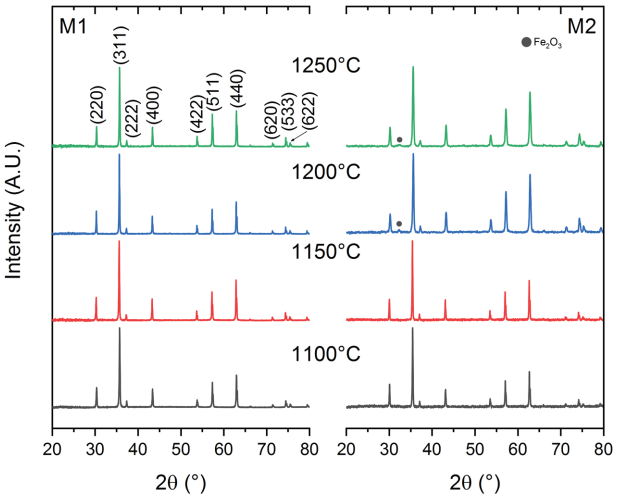

Fig. 1. XRD patterns of samples synthesized by M1 (left) and M2 (right) and sintered between 1100 °C and 1250 °C.

crystallizes in the cubic spinel structure of Fd3m space group, according to the previously reported data for $NiFe_2O_4$ (JCPDF N° 74-2081) and $CoFe_2O_4$ (JCPDF N° 79-1744).[7,16] Interestingly, in samples obtained by the M2 method and sintered at 1200 °C and 1250 °C, the small reflection at 33° can be assigned to the presence of Fe_2O_3 (JCPDF N° 39-1346), as it was also reported by other researchers.[17,18] This secondary phase was also observed by Winiarska *et al.* in ferrite ceramics synthesized by the sol–gel method.[18]

Figure 2 shows the SEM micrographs and the grain-size distributions of the samples, synthesized by both methods, and sintered at 1250 °C. Moreover, Tables 1 and 2 show the average grain size, and the experimental density and the corresponding densification percentages of all sintered samples, respectively. From the figure, it can be observed that the average grain size of samples obtained by M1 is larger than for the samples obtained by M2. The larger grain size found in the samples synthesized by the mechanochemically activated solid-state reaction method (Fig. 2 and Table 1) could be associated with both the initial particle size and the surface energy of the synthesized powders. Besides, in samples synthesized by method 2, the secondary phase formation (as the observed Fe_2O_3 presence) could modify the grain growth during the sintering process. Moreover, grain growth increases with sintering temperature in samples synthesized by M1, whereas the grain growth was restricted in samples obtained by M2.

In addition, from Table 2 an increase in the densification degree with the sintering temperature is registered. Generally, the densification degree of samples obtained by M1 is slightly higher than those observed for M2. Remembering that the mechanochemistry phenomenon is based on the fracture of the particles because of impacts of the milling media, remarkable amounts of structural defects generated during the mechanochemical process can reduce diffusion length and subsequently increase the rate of atomic diffusion.[19]

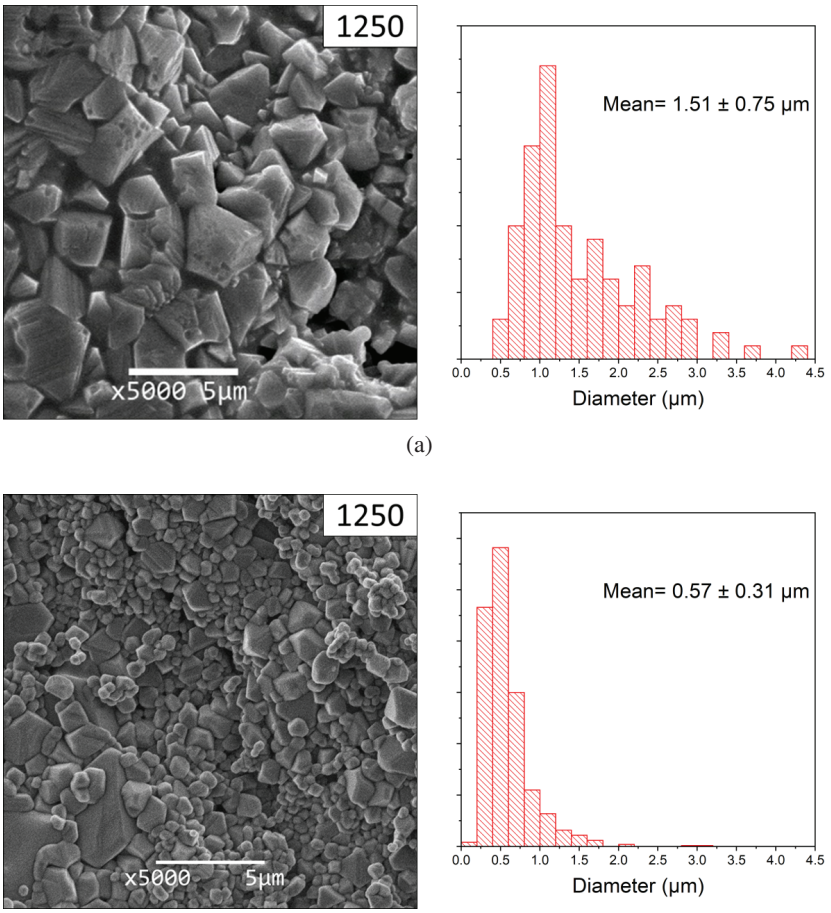

Fig. 2. SEM micrographs and grain-size distributions of samples synthesized by M1 (a) or M2 (b) and sintered at 1250 °C.

Table 1. Average grain-size values of sintered samples.

Sintering temperature [°C]	Average grain size (μm)	
	M1	M2
1100	0.54 ± 0.13	0.53 ± 0.19
1150	0.71 ± 0.26	0.60 ± 0.21
1200	0.79 ± 0.26	0.59 ± 0.24
1250	1.51 ± 0.75	0.57 ± 0.31

Table 2. Experimental density and densification percentage of sintered samples. Theoretical density is 5.36 g/cm^3.[20]

Sintering temperature [°C]	M1		M2	
	Density [g/cm³]	Densification [%]	Density [g/cm³]	Densification [%]
1100	4.85 ± 0.06	90.9	4.79 ± 0.06	89.8
1150	4.91 ± 0.07	92.0	4.77 ± 0.07	89.4
1200	4.94 ± 0.04	92.6	4.91 ± 0.06	92.0
1250	5.01 ± 0.05	93.9	4.97 ± 0.03	93.2

Therefore, powders synthesized by the mechanochemically activated solid-state method (M1) resulted in larger grains.

As an example, Fig. 3 shows the Raman spectrum of the NCF sample synthesized by M1 and sintered at 1100 °C. The presence of the five peaks associated with the characteristic Raman modes (A_{1g}, E_g, and $3T_{2g}$ modes) confirms the spinel phase formation in the sample.[21–23]

As shown in Fig. 3, the A_{1g} mode is the symmetric stretch of (Fe/M)–O bond (in tetrahedral coordination), whereas T_{2g} (2) mode is an anti-symmetric stretch. The E_g and T_{2g} (3) are symmetric and anti-symmetric bending modes of oxygen concerning Fe (M), respectively. The fifth mode, i.e., T_{2g} (1) corresponds to the translatory movement of the whole MO_4.[24] Considering that each Raman mode is related to a specific vibration and that different cations (Ni, Co, and Fe) can occupy the same position in the lattice, the contribution of the vibrations corresponding to each of the cations results in

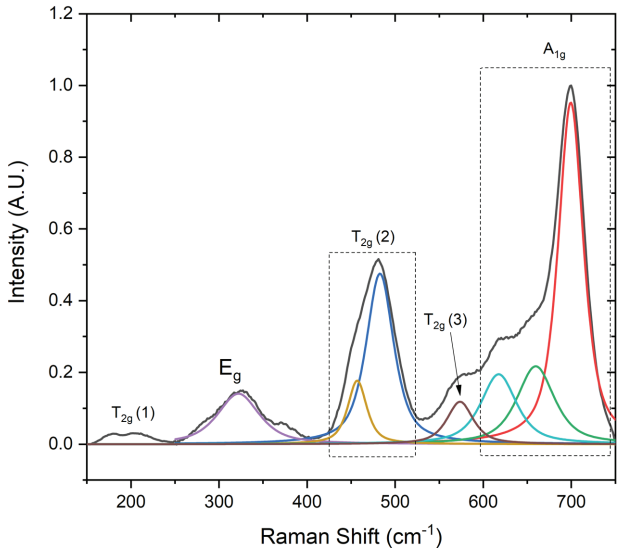

Fig. 3. Raman spectrum of NCF ceramic synthesized by M1 and sintered at 1100 °C with the deconvolution of the main bands.

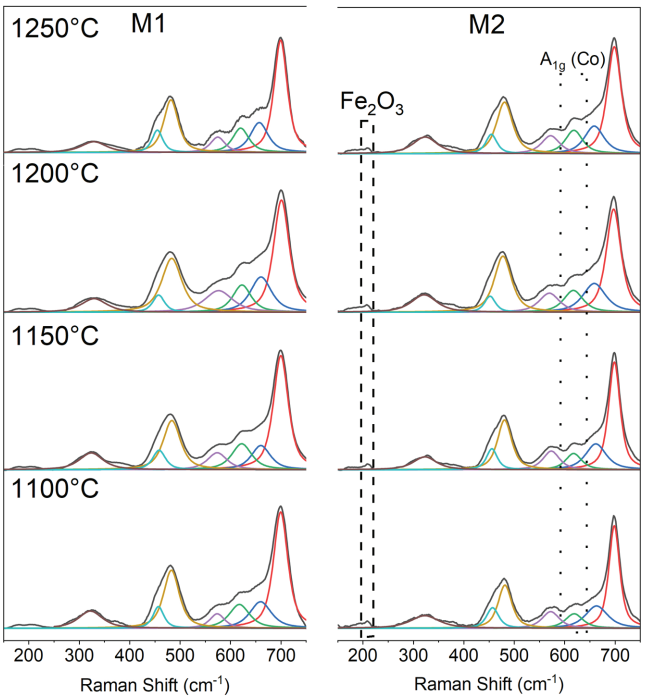

Fig. 4. Raman spectra of samples synthesized by M1 (left) and M2 (right) and sintered at temperatures ranging between 1100 °C and 1250 °C including the bands' deconvolution using Lorentzian functions.[24–26]

a wider band due to the influence of individual bands. This effect, due to the contribution of the bands generated by the cations (Fe, Ni, and Co), can be observed in the Raman spectrum between 600 cm^{-1} and 750 cm^{-1}. In particular, the band at 700 cm^{-1}, which includes two shoulders at 657 cm^{-1} and 620 cm^{-1}, can be assigned to the A_{1g} mode, while the remaining four bands are related to the T_{2g} (3), T_{2g} (2), E_g, and T_{2g} (1) modes. Moreover, according to previously published papers, the deconvolution of the A_{1g} band the most intense band at ~700 cm^{-1} is related to the Fe–O bonds, and the bands at 660 cm^{-1} and 620 cm^{-1} are associated with Fe–O and Co–O bonds, respectively.[25] The low intensity of the band assigned to the Ni–O bond hinders its complete deconvolution. The E_g and T_{2g} (3) modes correspond to the symmetric and antisymmetric bending of the oxygen atom in M–O bond at octahedral sites, respectively. Specifically, the overlapped bands close to 457 cm^{-1} and 482 cm^{-1} are assigned to the T_{2g} (2) mode of the nickel, cobalt, and iron at octahedral sites of the spinel structure. It is known that Co^{2+} forces the Fe^{3+} to migrate from the A-site to the B-site inducing the transformation of the nearly inverse spinel structure characteristic of the $NiFe_2O_4$ to a mixed spinel structure in NCF.[25] Furthermore, the displacement of the T_{2g} (3) mode can be related to defects in the sample (such as the presence of vacancies and interstitial cations or possible nonstoichiometries).[24] Finally, the T_{2g} (1) mode is observed for wavenumbers close to 200 cm^{-1}.

In Fig. 4, the spectra evolution of the sintered samples synthesized by both methods is presented. Interestingly, in samples synthesized by M2 a new peak at 150 cm^{-1} associated with A_{1g} mode of the Fe_2O_3 phase[26] is observed for the complete set of sintering temperatures. This peak indicates that the Fe_2O_3 secondary phase is formed in all the samples synthesized by M2 and it is only registered by XRD at the highest temperatures due to the increased crystallinity. Considering the A_{1g} band related to the Co–O bond, for samples synthesized by method 2, the increasing intensity with the sintering temperature could be attributed to the cobalt incorporation into the lattice displacing iron ions.

Figure 5 shows the magnetic hysteresis loops of the sintered samples. All the samples exhibited typical ferromagnetic behavior. Similar magnetic saturation (M_s) is observed for samples synthesized by both methods and sintered at 1000 °C and 1150 °C. However, for higher sintering temperatures, larger M_s values for samples synthesized by the solid-state route (M1) are registered. Taking into account that the reduction in particle size causes an increase in the proportion of the noncollinear magnetic structure on the particle surface layer, in which the magnetic moments are not aligned with the external magnetic field, the magnetic saturation behavior can be attributed to the increased grain growth in samples synthesized by M1 as observed in Table 1. Furthermore, as noted in other works,[15] the secondary phase content in samples synthesized by the Pechini method (M2) could also decrease the magnetic saturation. Although the coercive field decreased in all samples with the increase in sintering temperature, the samples obtained by M2 recorded the highest coercive values in the entire temperature range. Remembering that a combination of various microstructure factors such as grains or pores parameters, microstrain, impurities, or defects affects the values of H_c,[15] the observed behavior can be related to the

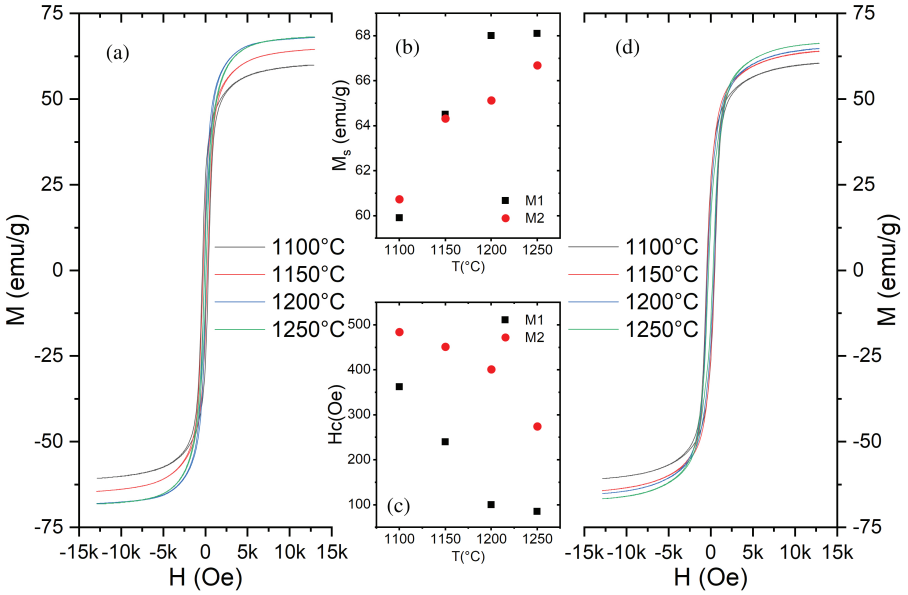

Fig. 5. Magnetic hysteresis loops, at room temperature, of NCF ceramics sintered between 1100 °C and 1250 °C. Method 1 (a), M_{max} versus sintering temperature (b) and H_c versus sintering temperature (c) comparative graphs, and Method 2 (d).

reduced grain growth, lattices parameters (stiffness and magnetocrystalline anisotropy) and the secondary phase presence in samples obtained from the Pechini's method which results in increase in pinning sites for the spins and could lead to an increased coercive field.

4. Conclusion

In this study, NCF magnetic ceramics were obtained using two alternative routes: solid-state reaction and Pechini's methods. The stabilization of the spinel structure was confirmed, by Raman and XRD techniques, in the full set of sintering temperatures studied. In samples synthesized by Pechini's method, Fe_2O_3 as a secondary phase was detected in all the sintered samples. Moreover, samples obtained by the solid-state reaction method presented improved magnetic properties (high magnetic saturation and low coercive field) due to the absence of secondary phases, and larger grain size than those obtained from Pechini's method. In conclusion, the solid-state reaction method, including the mechanochemical activation of the reagents, brings better results than Pechini's synthesis method for the complete sintering range.

Acknowledgments

The authors would like to thank National University of Mar del Plata (UNMdP) and National Scientific and Technical Research Council (CONICET) for providing financial support. The authors would like to thank Dr. Paula Bercoff for her advice on the magnetic measurements.

References

[1]X. Gao, L. Liu, B. Birajdar, M. Ziese, W. Lee, M. Alexe and D. Hesse, High-density periodically ordered magnetic cobalt ferrite nanodot arrays by template-assisted pulsed laser deposition, *Adv. Funct. Mater.* **19**, 3450 (2009).

[2]K. Ahalya, N. Suriyanarayanan and V. Ranjithkumar, Effect of cobalt substitution on structural and magnetic properties and chromium adsorption of manganese ferrite nano particles, *J. Magn. Magn. Mater.* **372**, 208 (2014).

[3]F. Bensebaa, F. Zavaliche, P. L'Ecuyer, R. W. Cochrane and T. Veres, Microwave synthesis and characterization of Co-ferrite nanoparticles, *J. Colloid Interface Sci.* **277**, 104 (2004).

[4]R. M. Mohamed, M. M. Rashad, F. A. Haraz and W. Sigmund, Structure and magnetic properties of nanocrystalline cobalt ferrite powders synthesized using organic acid precursor method, *J. Magn. Magn. Mater*. **322**, 2058 (2010).

[5]K. Maaz, S. Karim, A. Mumtaz, S. K. Hasanain, J. Liu and J. L. Duan, Synthesis and magnetic characterization of nickel ferrite nanoparticles prepared by co-precipitation route, *J. Magn. Magn. Mater*. **321**, 1838 (2009).

[6]A. Kumar, N. Yadav, D. S. Rana, P. Kumar, M. Arora and R. P. Pant, Structural and magnetic studies of the nickel doped $CoFe_2O_4$ ferrite nanoparticles synthesized by the chemical co-precipitation method, *J. Magn. Magn. Mater.* **394**, 379 (2015).

[7]A. Kumar, P. Sharma and D. Varshney, Structural, vibrational and dielectric study of Ni doped spinel Co ferrites: $Co_{1-x}Ni_xFe_2O_4$ (x = 0.0, 0.5, 1.0), *Ceram. Int.* **40**, 12855 (2014).

[8]M. S. Hossain, M. B. Alam, M. Shahjahan, M. H. A. Begum, M. M. Hossain, S. Islam, N. Khatun, M. Hossain, M. Saiful Alam and M. Al-Mamun, Synthesis, structural investigation, dielectric and magnetic properties of Zn^{2+}-doped cobalt ferrite by the sol–gel technique, *J. Adv. Dielect.* **8**, 1850030 (2018).

[9]A. Pradeep, P. Priyadharsini and G. Chandrasekaran, Sol-gel route of synthesis of nanoparticles of $MgFe_2O_4$ and XRD, FTIR and VSM study, *J. Magn. Magn. Mater.* **320**, 2774 (2008).

[10]S. G. Doh, E. B. Kim, B. H. Lee and J. H. Oh, Characteristics and synthesis of Cu-Ni ferrite nanopowders by coprecipitation method

with ultrasound irradiation, *J. Magn. Magn. Mater.* **272–276**, 2238 (2004).
[11]B. Baruwati, R. K. Rana and S. V. Manorama, Further insights in the conductivity behavior of nanocrystalline $NiFe_2O_4$, *J. Appl. Phys.* **101**, 014302 (2007).
[12]N. B. Velhal, N. D. Patil, A. R. Shelke, N. G. Deshpande and V. R. Puri, Structural, dielectric and magnetic properties of nickel substituted cobalt ferrite nanoparticles: Effect of nickel concentration, *AIP Adv.* **5**, 097166 (2015).
[13]A. B. Salunkhe, V. M. Khot, M. R. Phadatare and S. H. Pawar, Combustion synthesis of cobalt ferrite nanoparticles - Influence of fuel to oxidizer ratio, *J. Alloys Compd*. **514**, 91 (2012).
[14]H. Ahmadian Baghbaderani, M. R. Rahimipour and M. Delshad Chermahini, A combined experimental and modeling study of thermodynamics and kinetics of mechanochemical treatment for synthesis of $Ni_{0.5}Co_{0.5}Fe_2O_4$, *Mater. Des.* **95**, 54 (2016).
[15]M. Delshad Chermahini, H. Ahmadian Baghbaderani, M. M. Shahraki and M. Kazazi, Low temperature sintering of magnetic $Ni_{0.5}Co_{0.5}Fe_2O_4$ ceramics prepared from mechanochemically synthesized nanopowders, *Ceram. Int.* **45**, 5491 (2019).
[16]K. Maaz, S. Karim, K. J. Lee, M. H. Jung and G. H. Kim, Effect of temperature on the magnetic characteristics of $Ni_{0.5}Co_{0.5}Fe_2O_4$ nanoparticles, *Mater. Chem. Phys*. **133**, 1006 (2012).
[17]S. K. Mandal, S. Singh, P. Dey, J. N. Roy, P. R. Mandal and T. K. Nath, Temperature and frequency dependence of AC electrical properties of Zn and Ni doped $CoFe_2O_4$ nanocrystals, *Philos. Mag*. **97**, 1628 (2017).
[18]K. Winiarska, I. Szczygieł and R. Klimkiewicz, Manganese-zinc ferrite synthesis by the sol-gel autocombustion method. Effect of the precursor on the ferrite's catalytic properties, *Ind. Eng. Chem. Res.* **52**, 353 (2013).
[19]J. S. Forrester and G. B. Schaffer, The chemical kinetics of mechanical alloying, *Metall. Mater. Trans. A* **26**, 725 (1995).
[20]M. K. Kokare, N. A. Jadhav, Y. Kumar, K. M. Jadhav and S. M. Rathod, Effect of Nd^{3+} doping on structural and magnetic properties of $Ni_{0.5}Co_{0.5}Fe_2O_4$ nanocrystalline ferrites synthesized by sol-gel auto combustion method, *J. Alloys Compd*. **748**, 1053 (2018).
[21]B. Nandan and M. C. Bhatnagar, Structural, vibrational and magnetic properties of $Ni_{1-x}Co_xFe_2O_4$ ferrites, *AIP Conf. Proc.* **1675**, 030072 (2015).
[22]S. Thota, S. C. Kashyap, S. K. Sharma and V. R. Reddy, Cation distribution in Ni-substituted $Mn_{0.5}Zn_{0.5}Fe_2O_4$ nanoparticles: A Raman, Mössbauer, X-ray diffraction and electron spectroscopy study, *Mater. Sci. Eng. B* **206**, 69 (2016).
[23]R. Chen, W. Wang, X. Zhao, Y. Zhang, S. Wu and F. Li, Rapid hydrothermal synthesis of magnetic $Co_xNi_{1-x}Fe_2O_4$ nanoparticles and their application on removal of Congo red, *Chem. Eng. J*. **242**, 226 (2014).
[24]O.N. Shebanova and P. Lazor, Raman spectroscopic study of magnetite ($FeFe_2O_4$): A new assignment for the vibrational spectrum, *J. Solid State Chem.* **174**, 424 (2003).
[25]B. Nandan, M. C. Bhatnagar and S. C. Kashyap, Cation distribution in nanocrystalline cobalt substituted nickel ferrites: X-ray diffraction and Raman spectroscopic investigations, *J. Phys. Chem. Solids* **129**, 298 (2019).
[26]I. Chamritski and G. Burns, Infrared- and Raman-active phonons of magnetite, maghemite, and hematite: A computer simulation and spectroscopic study, *J. Phys. Chem. B* **109**, 4965 (2005).